JOURNAL OF COMPUTATIONAL PHYSICS 100, 409–418 (1992)

A Robust Elliptic Grid Generator

PATRICK M. KNUPP*

Ecodynamics Research Associates, Inc., P.O. Box 9229, Albuquerque, New Mexico 87119

Received September 19, 1990; revised May 17, 1991

A variational principle is proposed that results in a robust elliptic grid generator having many of the strengths of original Winslow or homogeneous Thompson–Thames–Mastin method (hTTM). The new grid generator places grid lines more uniformly over the domain than does hTTM, without loss of orthogonality. Numerically generated examples are given to demonstrate these effects. Grid quality measures are introduced to quantify differences between discrete grids. Both the hTTM and the new grid generator can generate folded grids on certain pathological regions, but overall they are very robust. Grid weighting for solution-adaptive calculations is briefly considered. Generalization of the new method to surface and volume grid generation is straightforward.

1. INTRODUCTION

Grid generation methods for boundary conforming coordinates are in widespread use, especially in computational fluid dynamics calculations (see, for example, [1, 2]). The present interest is in regular quadrilateral meshes for finite difference calculations. In this case, one seeks a mapping $(x(\xi, \eta), y(\xi, \eta))$ from the logical space $\{(\xi, \eta) \in [0, 1] \times [0, 1]\}$ to a planar physical domain defined by its bounding curves. The mapping should be smooth and have positive Jacobian. The Winslow [3] or homogeneous Thompson–Thames–Mastin (hTTM) equation [4] is perhaps the most robust automatic grid generator. The term robust is applied to reflect the fact that it can generate unfolded (one-to-one) grids on a wide variety of regions, while "automatic" refers to the fact that no arbitrary parameters are required. The method is based on the solution of the following pair of partial differential equations for the mapping functions x and y:

$$g_{22} x_{\xi\xi} - 2g_{12} x_{\xi\eta} + g_{11} x_{\eta\eta} = 0, \tag{1}$$

$$g_{22} y_{\xi\xi} - 2g_{12} y_{\xi\eta} + g_{11} y_{\eta\eta} = 0, \tag{2}$$

with

$$g_{11} = x_\xi^2 + y_\xi^2, \tag{3}$$

$$g_{12} = x_\xi x_\eta + y_\xi y_\eta, \tag{4}$$

$$g_{22} = x_\eta^2 + y_\eta^2. \tag{5}$$

The equations are generally solved as a Dirichlet problem, with boundary values obtained from the physical boundaries of the given domain.

There are several reasons for the popularity of this method. First, the homogeneous equations are of elliptic type, which guarantees a high degree of differentiability of the interior grid. Thus, for example, boundary-slope discontinuities are not propagated into the interior grid (an important feature not shared by algebraic or hyperbolic grid generation methods). Formulation of the grid generation problem in terms of an elliptic boundary value problem has a second strength, namely, that the interior grid is relatively independent of the boundary parameterization. As a result, the manner in which points are distributed along the given boundary is a secondary consideration. This property is a big advantage over grid generation methods which are highly sensitive to the positioning of the boundary points such as conformal mappings and orthogonal grid generators. The latter grid generators are based on ill-posed problems in which small changes in the boundary data can lead to large changes in the interior solution (and in many cases may preclude the existence of any solution at all).

Yet another strength of hTTM is that no arbitrary parameters are used; there is only one solution grid for each given region with fixed boundary parameterization. Therefore, the method is fully automatic. This is reinforced by the fact that the solution grid always exists (since the inverse mapping from physical to logical space is the solution of a pair of Laplace equations) and generally is one-to-one. Thus, hTTM users seldom need to intervene in the grid generation process to obtain an adequate grid.

In spite of the widespread success of the hTTM, some criticisms of the method have been made. First, it is well known that the solution grid lines are attracted towards

* This work was partially supported by the National Science Foundation Grant No. ISI-9061162.

0021-9991/92 $5.00

interior convexities and repelled from interior concavities. In other words, grid lines tend to be non-uniformly placed, being concentrated near the boundary in regions of compression and dispersed in regions of tension. The "non-uniformity" property of hTTM is a consequence of the grid satisfying Laplace equations on the physical domain [5]. Grid uniformity is an essential requirement of a non-solution adaptive grid generator in that there is no à priori reason to concentrate grid features into a particular portion of the given domain. Grid clustering is properly the function of a weighted (solution-adaptive) grid generator; such weighted systems should adapt away from a uniform grid created by a non-adaptive method.

A second criticism ([6] and others) is that the interior hTTM grid frequently lacks orthogonality. This is important because finite difference computations performed on non-orthogonal grids generally lead to larger truncation errors [7]. Inhomogeneous "P" and "Q" terms are introduced as a control mechanism for modifying the homogenous grid, but their meaning relative to orthogonality is unclear.

A third criticism is that in certain (admittedly rare) cases, the grid obtained from solving the discretized equations can be folded, i.e., the transformation is not always one-to-one (examples of folded grids produced by hTTM are given in [8]). The maximum principle has been invoked in proofs that the analytic transformation is one-to-one [9]; apparently, the discrete equations do not preserve this highly desirable property.

In spite of these drawbacks, the hTTM method is perhaps the most widely known automatic grid generation method. Most other grid generation methods suffer from at least some of the same set of defects listed above (non-orthogonality, folded grids produced on highly non-convex domains, do not have geometric interpretations) or lack automation, ellipticity, or fail to exist except on limited classes of regions. In this paper a new method of grid generation (referred to as AO for "area-orthogonality") is proposed. It is a viable alternative to hTTM, having many of the strengths of hTTM and in some cases, at least, overcomes the latter's weaknesses. As an added attraction, it has ready generalizations to surface and volume grid generation.

2. THE AREA-ORTHOGONALITY GRID GENERATOR

The area-orthogonality (AO) grid generator is a special case of the more general variational grid generation system formulated by Steinberg and Roache [10]. The primary feature of the latter is that the variational grid generator is posed in terms of mappings $x = x(\xi, \eta)$, $y = y(\xi, \eta)$ from the logical space to the physical space (in contrast to the Brackbill and Saltzman variational method [11] which maps physical domains to logical space). The main advantage of the Steinberg–Roache method over the Brackbill–Saltzman is that the former permits direct control over geometric grid qualities as smoothness, area, and "orthogonality." Numerical experiments using the Steinberg–Roache equations have shown that for difficult domains (such as those which are highly non-convex), it is unusual for any single grid quality to suffice by itself in generating an adequate grid. For such domains one generally employs weighted combinations (w_s, w_a, w_o) of *smoothness*, *area*, and *"orthogonality."* The resultant combined functional can be written

$$I_w = \int_0^1 \int_0^1 [w_s(g_{11} + g_{22}) + w_a g + w_o g_{12}^2] \, d\xi \, d\eta \quad (6)$$

with

$$g = g_{11} g_{22} - g_{12}^2. \quad (7)$$

The weighted functional I_w contains the three parameters w_s, w_a, and w_o which the user must select in order to determine the grid. Although such a weighted functional gives one considerable flexibility (adequate grids can be obtained on most domains through trial and error), it saddles one with the chore of choosing the parameters. In contrast, hTTM and AO are automatic. There are dangers in using the weighted grid generator blindly; some choices of the parameters lead to partial differential equations having no solution for the given domain. Full 'orthogonality" weighting (0, 0, 1) is a good example, since it is not possible to place orthogonal grids on arbitrary domains, particularly if the boundary parameterization is already given. Attempts to solve the pure "orthogonality" equations on an arbitrary domain will result in convergence failure when using an iterative solver. Another only slightly less serious problem of the weighted grid generator is that some combinations of the weights do not lead to elliptic grid generators. Full area weighting (0, 1, 0) is a prime example. The resulting grids are not necessarily smooth. Considerable effort has been expended to find a subset of the full parameter range that works well on a wide variety of domains. A mixture of *smoothness* and *area* $(w_s, w_a, 0)$ was proposed to obtain smooth, unfolded grids [12]. Several examples were given to show that this works reasonably well. Recent theoretical work [17] demonstrates that this particular combination of weights (with $w_s \neq 0$) results in an elliptic grid generator. Although the mixture of *smoothness* and *area* is quite useful, one still must supply two parameters.

This work identifies AO as another useful combination of the weights (not previously studied by the authors of [12]) which deserves special attention. The combination is distinctive for several reasons. First, it results in an elliptic grid generator. Somewhat surprisingly, ellipticity is achieved

without the use of *smoothness*. Second, the generator has no arbitrary parameters, making it an "automatic" method. Third, the resulting grids are generally quite satisfactory, giving near-orthogonal and near-equal area grids on a wide variety of domains. The grids do not have the well-known property of attraction to concavities shared by both *smoothness* and hTTM. Finally, the equations are simpler than those obtained by the *smoothness–area* combination and require less storage. The method is not a panacea, but should be viewed as a useful alternative to hTTM or to *smoothness–area*.

A reviewer has questioned whether the presently proposed AO method is really "new," since it is a special case of the "known" Steinberg–Roache method of variational grid generation. However, Steinberg and Roache themselves disagree [18], noting that their analysis and tests of their general formulation, with three independently adjustable parameters, gave no suggestion regarding the particular features and advantages of the present AO method. Furthermore, based on the insight developed from their numerical experimentation [12], the AO method would have been rejected à priori [18].

The proposed AO method is obtained from the combined weighting functional I_w by the triple $(0, \frac{1}{2}, \frac{1}{2})$. The functional is

$$I_{AO}[x, y] = \tfrac{1}{2}\int_0^1 \int_0^1 g_{11}\, g_{22}\, d\xi\, d\eta. \tag{8}$$

There is no straightforward geometric interpretation of this functional; it is halfway between the equal-area grid and the "orthogonal" grid resulting from the minimization of g_{12}^2. AO is automatic since, like hTTM, there are no arbitrary weights or parameters in the functional.

The AO Euler–Lagrange equations have the convenient form

$$\mathscr{L}x = 0, \tag{9}$$

$$\mathscr{L}y = 0, \tag{10}$$

with

$$\mathscr{L} = \frac{\partial}{\partial \xi} g_{22} \frac{\partial}{\partial \xi} + \frac{\partial}{\partial \eta} g_{11} \frac{\partial}{\partial \eta}. \tag{11}$$

The resulting partial differential equations are clearly elliptic (except in the degenerate cases g_{11}, $g_{22} = 0$). This is rather surprising, since they are derived without any weighting toward *smoothness*. Nevertheless, the smoothness property of elliptic grid generators is expected from solutions to these equations and is verified in the computational section to follow.

The fully expanded form of the AO Euler–Lagrange equations bears a strong resemblance to the hTTM equations:

$$g_{22} x_{\xi\xi} + 4x_\xi x_\eta x_{\xi\eta} + g_{11} x_{\eta\eta} + 2(x_\xi y_\eta + x_\eta y_\xi) y_{\xi\eta} = 0, \tag{12}$$

$$g_{22} y_{\xi\xi} + 4y_\xi y_\eta y_{\xi\eta} + g_{11} y_{\eta\eta} + 2(x_\xi y_\eta + x_\eta y_\xi) x_{\xi\eta} = 0. \tag{13}$$

Only the cross derivative terms differ from those which occur in hTTM. This suggests that the method should share many of the properties of hTTM, a fact borne out by the numerical experiments described next.

3. NUMERICAL RESULTS

3.1. *Comparison with hTTM Grids*

Although no mathematical proofs concerning the behavior of the AO method are yet known, numerical evidence suggests that a very robust grid generator results from the solution of Eqs. (12)–(13). Figures 1, 2, and 3 compare grids generated by the hTTM and the AO method on several difficult domains. A number of other domains were tried with similar results, but are not included to save space. Visual examination of the figures suggests that AO grids are smooth, as expected from the elliptic operator. This is most evident in Figure 2 which involves a domain having a boundary-slope discontinuity on the top and bottom boundaries. An especially important observation is that AO grid lines appear to enter concave portions of the domains much more so than does hTTM. In general, grid lines in AO appear to cover the domain more uniformly than hTTM (especially in Figs. 1 and 3). AO does so without loss of

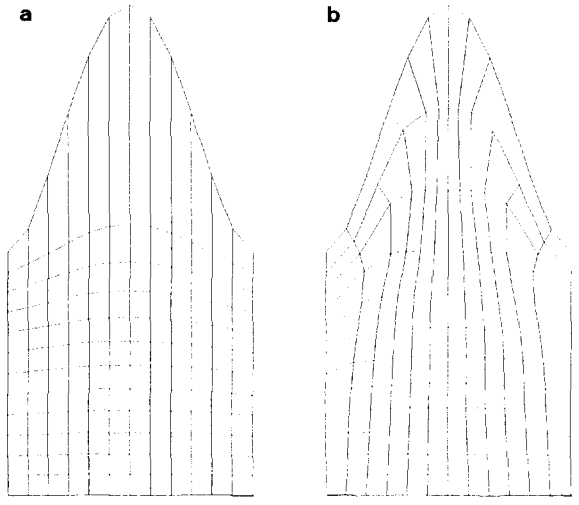

FIG. 1. Comparison of hTTM and AO on a "house-like" domain.

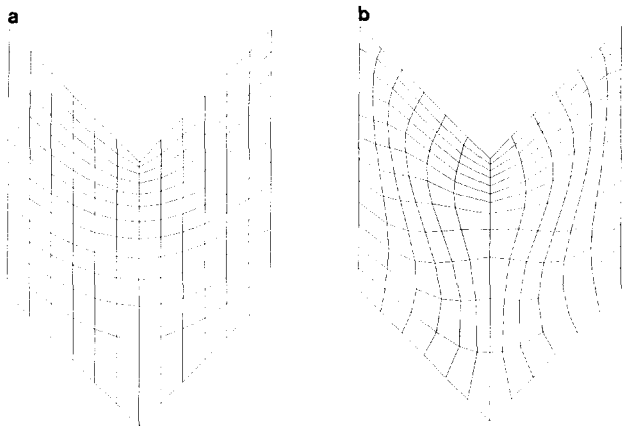

FIG. 2. Comparison of hTTM (a) and AO (b) on a "V-shaped" domain.

orthogonality; in some cases the overall orthogonality is even increased. There is no provision in either method for controlling orthogonality on the boundary. This is simultaneously a strength and weakness because, by not requiring truly orthogonal grids, the problem of computing the proper boundary point distribution is avoided. Even on the boundary, however, the AO grid frequently appears more nearly orthogonal than the corresponding hTTM grid.

An attempt was made to confirm these visual impressions by using quantitative measures. Although it is difficult to compete with the information-processing capabilities of the human eye, a compatible set of quantitative measures can confirm or dispute one's impression and perhaps identify grid features overlooked by casual visual assessments. The quantitative measures adopted here were carefully selected from numerous candidates for their ability to quantify the visual impression of Figs. 1–3. Since the final product in grid generation is a discrete grid, rather than a continuum mapping, the measures are based on discrete, rather than continuous quantities. The measures adopted here highlight grid flaws instead of grid quality because it is easier to detect poor features of a given grid than it is to state what constitutes a "good" grid. Three general types of grid flaws have been identified, namely, grids that (i) lack smoothness, (ii) have folded cells, or (iii) lack uniformity (of cell areas and/or angles). The smoothness property is not quantified here, since this is difficult and because the grids that are being compared should be smooth according to the theory of elliptic operators. Grids having folded cells are easily detected by taking the cross-product (in the right-hand sense) of any two adjacent cell-side vectors [8]. Let $\hat{k}$ be the unit normal perpendicular to the plane ($\hat{k} = \hat{\imath} \times \hat{\jmath}$). Then, if $\hat{k} \cdot (\mathbf{v}_1 \times \mathbf{v}_2) \leqslant 0$ for any of the four adjacent cell side-vectors (Fig. 4), the cell is considered folded (i.e., not convex). Grids with such cells are generally considered unsuitable for computational purposes. There is no need to apply the following uniformity measures to such grids.

Grid uniformity is more difficult to define, but is important in comparing smooth, unfolded grids. Two discrete quantities of interest are the cell areas and the cell angles. The areas are computed from $A_k = \frac{1}{2}\hat{k} \cdot [\mathbf{v}_1 \times \mathbf{v}_2 + \mathbf{v}_3 \times \mathbf{v}_4]$. Rather than measure the cell angle θ, one can compute the deviation of the angle from orthogonality by $\phi = |\pi/2 - \theta|$. The angle θ may be computed from the relations

$$\mathbf{v}_1 \cdot \mathbf{v}_2 = \|\mathbf{v}_1\| \, \|\mathbf{v}_2\| \cos \theta, \tag{14}$$

$$\hat{k} \cdot (\mathbf{v}_1 \times \mathbf{v}_2) = \|\mathbf{v}_1\| \, \|\mathbf{v}_2\| \sin \theta. \tag{15}$$

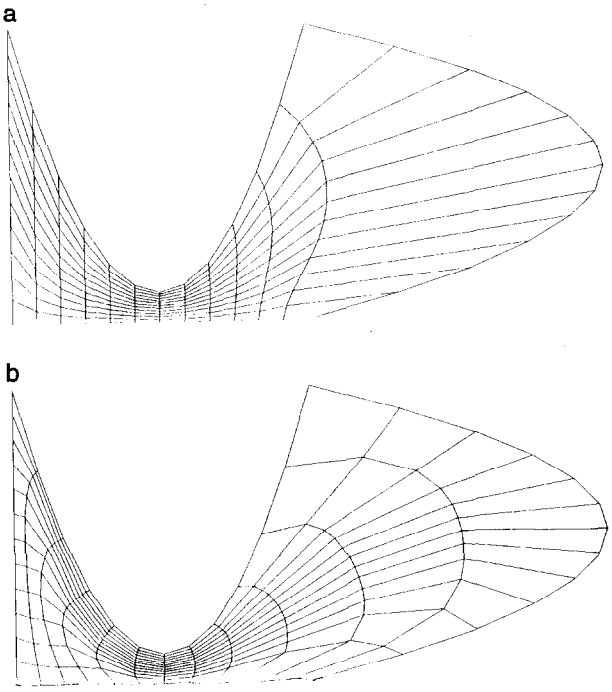

FIG. 3. Comparison of hTTM (a) and AO (b) on a "swan-like" domain.

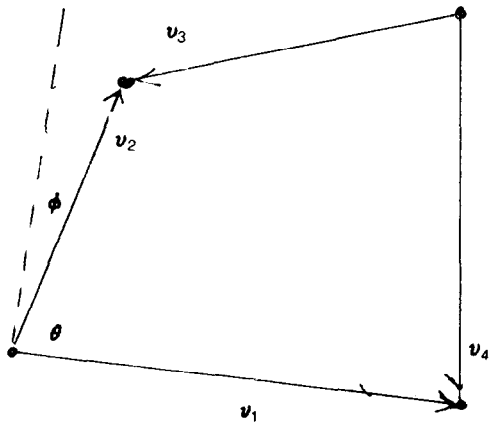

FIG. 4. Cell angles and areas used in grid quality measures.

TABLE I

Comparison of hTTM and AO Measures for Fig. 1 Grid

	hTTM angles	AO angles	hTTM areas	AO areas
Mean	8.0	11.0	0.011	0.011
S.D.	12.7	13.3	0.012	0.004
Max	72	58	0.072	0.025

A grid having M by N cells contains MN areas and $4MN$ angles, both being fairly large numbers even for small grid sizes. It therefore makes sense to study the discrete uniformity measures in terms of their statistical distribution, i.e., their mean, standard deviation, minimum, and maximum. Inferior grids will generally have larger means, a larger standard deviation, or perhaps a larger outlier indicated by the maximum angle-deviation or cell area. Since it only takes one or two bad angles to negate an otherwise good grid, the maximum angle-deviation is particularly important. Minimum values of the distribution are seldom significant, except when the minimum cell area is close to zero.

Tables I, II, and III give the uniformity measures computed for the grids shown in Fig. 1–3. The mean angle-deviation ϕ for the domain of Fig. 1 is 8° for the hTTM grid and 11° for the AO grid. The standard deviations of the angle distributions are similar for both methods. From this limited information one might erroneously conclude that the hTTM grid is superior. However, the maximum (worst-case) angle-deviation is 72° degrees for the hTTM grid and only 58° for the AO grid. Furthermore, the area measures show the AO grid to be better, since the area standard deviation and area maximum is significantly smaller in the AO grid. The quantitative measures thus refine and confirm the visual impression one obtains from Fig. 1, namely that the hTTM grid contains excessively large cells on the top row of the grid. The area mean is the same for both methods, as must be true for any grid on a fixed domain with fixed boundary points [15].

Table II compares the grid "metrics" on the "V-shaped" domain of Fig. 2. In this example, the AO angle-deviation measures of the mean and standard deviation are smaller than those of hTTM. This feature shows up even more strongly in Fig. 5, which plots histograms of the grid angle-deviation and area distributions for both methods. The hTTM angle-deviation histogram contains considerably more angles near 45° than does AO. The few AO angles that are 45° are the result of the symmetry requirement imposed by the domain, rather than the result of a deficiency of the method. Area outliers are less prominent in the AO grid as can be seen in both Table II and the histogram plot. The uniformity measures given in Table III exhibit a similar pattern on the third domain.

TABLE II

Comparison of hTTM and AO Measures for Fig. 2 Grid

	hTTM angles	AO angles	hTTM areas	AO areas
Mean	28.6	20.6	0.007	0.007
S.D.	12.2	9.5	0.003	0.003
Max	45	45	0.024	0.015

TABLE III

Comparison of hTTM and AO Measures for Fig. 3 Grid

	hTTM angles	AO angles	hTTM areas	AO areas
Mean	29.1	19.9	0.007	0.007
S.D.	20.9	15.1	0.016	0.010
Max	80	75	0.073	0.066

A resolution study was undertaken for the first domain to observe the behavior of the uniformity measures as one approaches the continuum transformation. Results are given for the angle-deviation in Table IV and for the cell areas in Table V. Both methods fare poorly on reducing the maximum angle-deviation measure. Although the mean and standard deviation of the angles decreases, the maximum angle-deviation (worst-case outlier) does not improve with grid resolution. The area-uniformity measures in Table V are multiplied by the number of cells (N^2) to keep the mean constant. With this correction applied, it is apparent that the hTTM area standard deviation and area maximum increase with increased resolution, whereas they remain relatively constant in AO. This indicates that the excessively large cells generated in hTTM are not eliminated by increased grid resolution.

3.2. *Grid Folding on a Pathological Domain*

Both methods appear to be very robust in that the grids are not folded even on many highly non-convex domains (Fig. 3, for example). However, it is possible to produce folded grids using either hTTM or AO. The horseshoe domain in Fig. 6 was previously used to show that the discrete hTTM grid can be folded [8], despite claims to the contrary for the continuum mapping [7]. The domain consists of two concentric ellipses having eccentricity as a parameter. The eccentricity is here measured in terms of the "aspect ratio" r which is defined as the ratio of the major and minor axes. Figures 6a, b, and c were produced by hTTM on regions having aspect ratios 4.0, 4.43, and 5.0, respectively. In 6a, the hTTM grid is highly non-uniform, a prelude to folding. In 6b folding becomes quite evident (at $r = 4.40$, the grid was barely unfolded). A relatively small increase in aspect ratio to $r = 5.0$ (Fig. 6c) results in a catastrophic collapse of the hTTM grid lines. This is perhaps indicative of ill-possedness or solution bifurcation. As noted in [8], an increase in grid resolution raises the

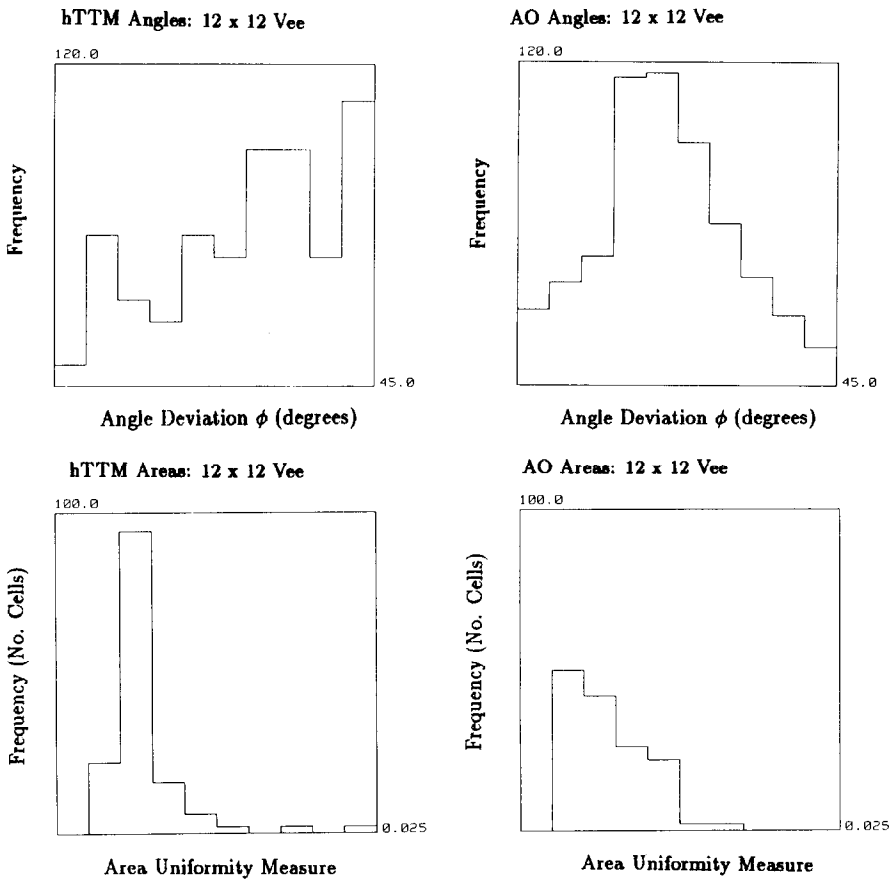

FIG. 5. Histograms for uniformity measures on the "V-shaped" domain.

critical aspect ratio, but apparently not fast enough to avoid the possibility of folding even under high resolution. This pattern is confirmed in Table VI.

Figures 6d, e, and f show the corresponding grids generated by AO for the same aspect ratios. Even for $r = 5.0$, the AO grid remains unfolded. However, it is quite possible for AO to produce a folded grid. Critical aspect ratios for AO are again given in Table VI for the horseshoe region. For a fixed grid resolution, significantly larger aspect ratios are needed to produce a folded grid using AO compared to hTTM. In addition, 8×8 and 16×16 grids were computed on the horseshoe domain with an aspect ratio of 50 using AO. The solution grids did not undergo catastrophic collapse as in Fig. 6c even though the grids were folded.

It appears from these experiments, at least, that AO is more robust to folding than hTTM. However, this is not always true. Figure 7a gives an example in which the AO grid generator gives a folded grid on a domain for which hTTM has no trouble. Reparameterization of the top boundary in 7b is sufficient to correct the problem in this case, but this example shows that AO is not a solution to the folding problem.

TABLE IV

A Resolution Study on the Angle Uniformity Measure

$N \times N$	hTTM			AO		
	Max	S.D.	Mean	Max	S.D.	Mean
5	69	9.7	16.2	65	14.5	16.9
10	71	8.4	13.4	58	11.9	14.5
20	72	7.6	11.3	62	10.0	11.5
40	72	7.9	10.8	71	9.0	10.1

TABLE V

A Resolution Study on the Area Uniformity Measure

$N \times N$	hTTM			AO		
	Mean	S.D.	Max	Mean	S.D.	Max
5	1.525	1.025	4.9	1.525	0.525	2.7
10	1.525	1.525	8.9	1.525	0.600	3.3
20	1.525	2.000	16.0	1.525	0.800	4.0
40	1.525	3.200	27.2	1.525	0.800	3.2

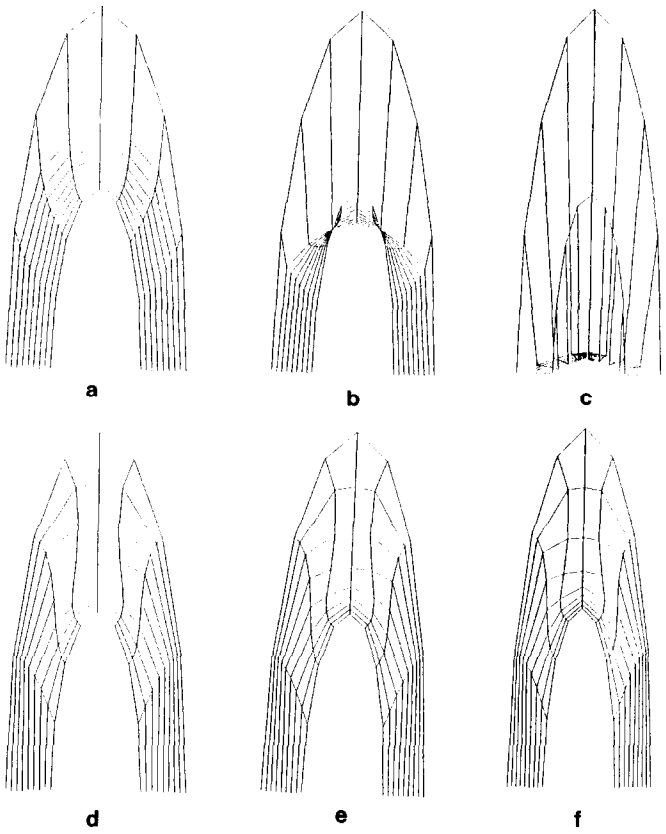

FIG. 6. Comparison of hTTM and AO folding on a horseshoe domain: (a) hTTM, $r=4.0$; (b) hTTM, $r=4.43$; (c) hTTM, $r=5.0$; (d) AO, $r=4.0$; (e) AO, $r=4.43$; (f) AO, $r=5.0$.

If one inverts the AO equations (12)–(13), by expressing them on the physical domain, one does not obtain a Laplace equation but rather a very complex nonlinear equation; i.e., it is not clear that the maximum principle can be invoked in proofs of monotonicity. Considerable theoretical work will be needed to account for the robustness of this functional and to determine the conditions under which a one-to-one transformation can be guaranteed.

3.3. *Weighted Combinations of Area and Orthogonality*

Generalization of AO to the weighted combination $(0, w_a, w_o)$ is not advocated because the Euler–Lagrange equations are no longer necessarily elliptic; terms of the form $(\partial/\partial\xi)\ g_{12}(\partial/\partial\eta)+(\partial/\partial\eta)\,g_{12}(\partial/\partial\xi)$ appear in the operator. However, it can be shown that the condition $0<\beta<2$ with $\beta=w_o/w_a$ guarantees ellipticity. Numerical experiments were performed on the horseshoe domain (critical aspect ratio of 4.0) for various values of β, with $\beta=1$ giving the basic AO method. Grid uniformity measures for these calculations are given in Table VII. Somewhat surprisingly, the angle-deviation measures did not decrease monotonically with increasing β as one would expect (since one is moving toward *"orthogonality"*). The optimal β appears to be near 1.5.

TABLE VI

Horseshoe Critical Aspect Ratio vs Grid Resolution

Critical	Aspect	Ratio
$N\times N$	hTTM	AO
2	2.15	2.45
4	4.55	10.25
8	4.42	15.36
16	4.90	18.25
32	<5.5	>20.0

This behavior is explained by the fact that minimization of g_{12}^2 does not lead to the "scaled-Laplacian" equations [6] for orthogonal grids, but to another set having a somewhat different geometrical meaning. As expected, the area measures do decrease monotonically as β decreases (except, of course, for the area mean). Grids produced with $\beta=0.1$ and 2.5 were folded.

Although superior grids can sometimes be produced by values of the parameter β other than unity, AO remains a good compromise between area and *"orthogonality."* Furthermore, AO is attractive because the automatic feature is lost by the introduction of the parameter β and by the fact that folded grids occur with greater likelihood. Frankly, in the absence of evidence to the contrary, one is loath to depart from $\beta=1$, since the resemblance of the Euler–Lagrange equations to the hTTM equations is blurred.

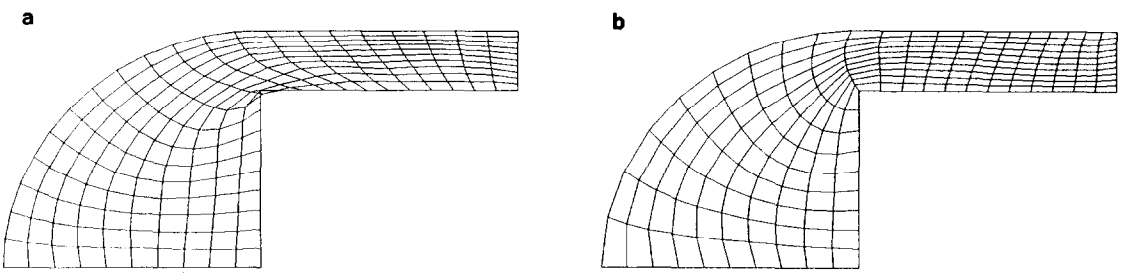

FIG. 7. A folded AO grid: (a) natural boundary parameterization; (b) stretched boundary parameterization.

TABLE VII

Comparison of Weighted Area-Orthogonality Measures on Fig. 5 Grid

β	Angles			Areas		
	Mean	S.D.	Max	Mean	S.D.	Max
0.1	37	19	75	0.129	0.013	0.151
0.5	31	18	73	0.129	0.040	0.239
1.0	29	17	68	0.129	0.063	0.316
1.5	27	16	62	0.129	0.084	0.373
2.0	28	18	77	0.129	0.104	0.427

3.4. *AO Performance*

To achieve symmetric grids on symmetric objects, Eqs. (12)–(13) were solved using centered finite difference approximations for all the partial derivatives. The difference equations were linearized by lagging the first-order coefficients, with updating occurring every NSMO (number of smoothings per coefficient update) Gauss–Seidel sweeps of the linearized system of equations. Since the present objective is to examine the quality of the grids produced by the AO method, a relatively inefficient linear solver was deemed adequate. For production codes, one would want to consider faster solvers such as multigrid or conjugate gradient.

In general, for a fixed value of NSMO, approximately twice as many coefficient updates were needed to obtain iterative convergence to the solution with the AO method than were needed for hTTM. However, for especially difficult domains (such as the horseshoe), AO required fewer updates than hTTM. There is a trade-off between updating the coefficients and continued smoothing in the Gauss–Seidel iteration; if NSMO is too small, too many operations are used to calculate updated coefficient arrays; if NSMO is too large, too many operations are devoted to smoothing with inaccurate coefficients. Therefore, there is an optimal (domain dependent) value for NSMO. It was found that for convex or nearly convex domains, one does not need to update the lagged coefficients as frequently as for highly non-convex regions. For the nearly convex domains, the optimal NSMO is about 9 to 13. For highly non-convex domains, NSMO should be set in the range 3 to 6.

Five arrays are required to store the lagged-coefficient data in AO, compared to three with hTTM. This is not considered a significant storage penalty in view of the apparent gain in grid quality. In comparison, nine coefficient arrays are needed to implement the full variational method derived from (6) and also the method involving weighted combinations of *area* and *"orthogonality"* used in Section 3.3.

Direct differencing of the Euler–Lagrange equations (9)–(10) was also tried, but with disappointing results. The grids produced were nearly identical to those produced by differencing the fully expanded equations (12)–(13), but coefficient updating was required approximately twice as much as in the solution of (12)–(13). Further, the approach appears less robust in that grid folding occurs for significantly smaller values of the horseshoe critical aspect ratio.

4. WEIGHTED AO

Solution-adaptive calculations are possible using the AO grid generator. This is accomplished by adding a weighting function to adapt away from the uniform AO grid. The basic method is put forth in [10], wherein one weights the previous functional by the user-defined weight function $w(\xi, \eta)$ defined over the logical space, giving

$$I[x, y] = \int_0^1 \int_0^1 \frac{g_{11}\, g_{22}}{w}\, d\xi\, d\eta. \tag{16}$$

The Euler–Lagrange equations become

$$\mathscr{L}x = \frac{w_\xi}{w} g_{22} x_\xi + \frac{w_\eta}{w} g_{11} x_\eta, \tag{17}$$

$$\mathscr{L}y = \frac{w_\xi}{w} g_{22} y_\xi + \frac{w_\eta}{w} g_{11} y_\eta. \tag{18}$$

The right-hand side of these equations do not take the form of an inhomogeneous "source" term as in the inhomogeneous TTM method with its "P" and "Q" terms.

Weighted AO has the potential of achieving both point and line attraction. An example of point attraction is given in Fig. 8.

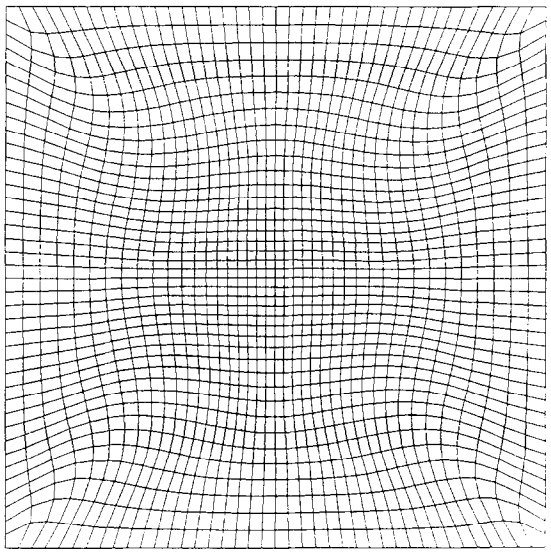

FIG. 8. Point attraction using AO.

The weight used was $w(\xi, \eta) = \exp(\lambda r^2)$ with $\lambda = 4$ and $r^2 = (\xi - 0.5)^2 + (\eta - 0.5)^2$.

The weight w can be made more useful by introducing the reference space concept used in [10]. The map $\alpha = \alpha(\xi, \eta)$, $\beta = \beta(\xi, \eta)$ defines a non-uniform grid on the unit square having properties similar to those desired for the grid on the physical domain. To form the weight w in (17)–(18), set $\tau_{11} = \alpha_\xi^2 + \beta_\xi^2$ and $\tau_{22} = \alpha_\eta^2 + \beta_\eta^2$. We take $w = \sqrt{\tau_{11}\tau_{22}}$. Details of the derivation are given in [10, 13]. It is important to note that the reference grid determines the boundary point distribution as well as the interior grid. Once the reference grid is chosen, boundary points are computed from the boundary parameterization and then held fixing during the solution of the grid generation partial differential equations.

This approach was used to construct the weighted grids in Fig. 9 and 10. Figure 9a shows a uniform reference grid ($\alpha = \xi$, $\beta = \eta$) having 40×8 cells (i.e., the unweighted case). Figure 9b shows the resulting unweighted AO grid. It is easy using the reference space conept to weight the grid toward smaller cells near the airfoil surface. Figure 9c shows a reference grid with smaller cells on the bottom edge, which corresponds to the surface of the airfoil. Additional weighting is obtained by concentrating smaller cells near the $\alpha = \frac{1}{2}$ line, which corresponds to the region in front of the leading edge of the airfoil. Figure 9d shows the resulting weighted grid in physical space to have the desired characteristics.

Figure 10 involves a domain similar to that which might occur in calculating flow over a "backstep." The uniform reference grid (40×10 cells) in Fig. 10a results in the unweighted AO grid on the backstep shown in Fig. 10b. It is desired to concentrate points closer to the bottom edge of the backstep, so the reference grid in Fig. 10c reflects that

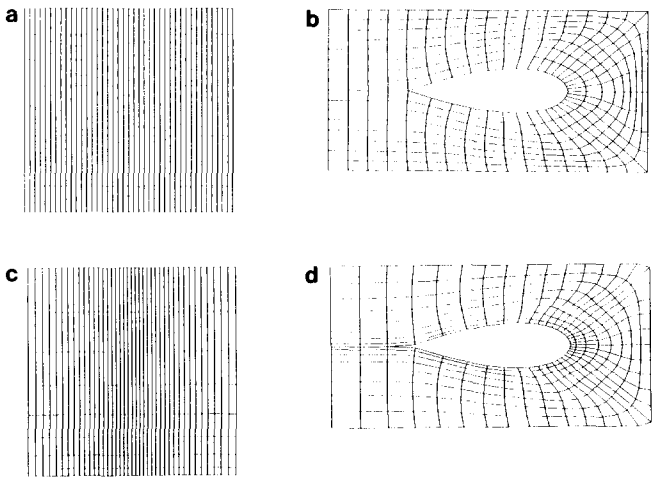

FIG. 9. AO weighted grid on an "airfoil": (a) reference grid (unweighted); (b) AO grid (unweighted); (c) reference grid (weighted); (d) AO grid (weighted).

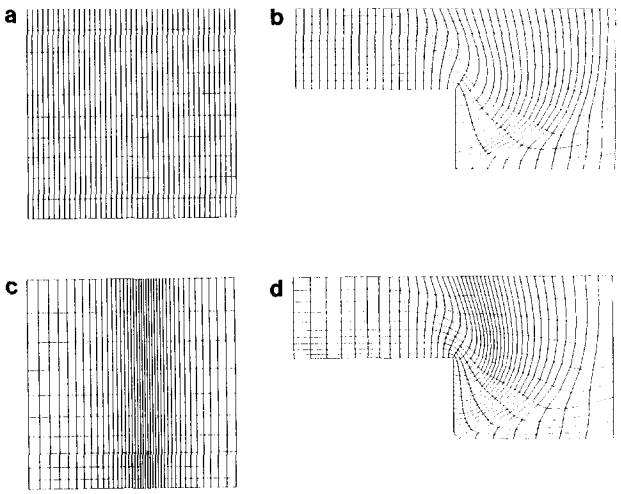

FIG. 10. AO weighted grid on a "backstep": (a) reference grid (unweighted); (b) AO grid (unweighted); (c) reference grid (weighted); (d) AO grid (weighted).

requirement. Also, points are concentrated to the $\alpha = 0.6$ line in reference space to obtain more grid lines near the step. The weighted grid in Fig. 10d is clearly an improvement over the unweighted grid.

These examples demonstrate how one can readily adjust the reference grid to obtain general features in the physical grid. Although the examples do so, one need not be restricted to the special case $w = \alpha(\xi)\,\beta(\eta)$. Alternatively, one could use the hybrid poisson adaptive scheme [16] to adapt away from the "base grid" obtained from the present unweighted method.

5. SUMMARY AND FUTURE EXTENSIONS

The examples given show the AO method to be a viable alternative to other grid generation methods. It is fully automatic with no scalar parameters to adjust. The computed grids exhibit elliptic behavior, i.e., discontinuities on the boundary do not propagate into the interior and the grid is relatively insensitive to the boundary parameterization. The grids exist for a wide range of domains including ones that are highly non-convex. These advantages are shared with the hTTM method. In addition, AO may often have the following additional advantages: (i) the interior grid may be more nearly orthogonal, (ii) the grid lines follow and extend into boundary concavities, (iii) the grids do not fold on a wide class of domains (as indicated by the experiments performed on the horseshoe domain). In addition, the AO method has a useful variational formulation which allows easy control of the grid by a weight function having a quasi-geometric meaning.

Finally, from a practical point of view, the strong resemblance of the AO equations to those of hTTM makes it a

relatively simple matter to include AO within existing grid generation software already having an hTTM option.

Evidence presented here in favor of AO is mostly numerical. In the future, one hopes for mathematical proofs of existence and uniqueness of solutions to the set of Eqs. (9)–(10). Mathematical results concerning the positivity of the Jacobian of the transformation are also highly desirable.

The author has recently proposed [14] a new grid generation methodology for robust surface grid generation which is already applicable to hTTM, *smoothness*, and *area* grid generators. The AO method has been incorporated as well. The relevant equations will be described in a future publication.

The generalization of AO method to three-dimensional volumes is clear. One uses the functional

$$I[x, y, z] = \int_0^1 \int_0^1 \int_0^1 \frac{g_{11}\, g_{22}\, g_{33}}{w}\, d\xi\, d\eta\, d\zeta. \tag{19}$$

The Euler–Lagrange equations for this case reads $\mathscr{L}x = 0$, $\mathscr{L}y = 0$, and $\mathscr{L}z = 0$ with

$$\mathscr{L} \equiv \frac{\partial}{\partial \xi}\left(g_{22}\, g_{33} \frac{\partial}{\partial \xi}\right) + \frac{\partial}{\partial \eta}\left(g_{11}\, g_{33} \frac{\partial}{\partial \eta}\right) + \frac{\partial}{\partial \zeta}\left(g_{11}\, g_{22} \frac{\partial}{\partial \zeta}\right). \tag{20}$$

Numerical investigations as to the quality of the resulting grids are planned for a future publication.

Finally, the direct variational method of planar grid generation [15] can also make use of the AO approach. The discrete analogue of the functional (6) is

$$F = \sum_n (l_1^2 + l_3^2)(l_2^2 + l_4^2), \tag{21}$$

where the sum is over all grid nodes and the l_k are the surrounding lengths of the line segments connecting to the node. Preliminary experiments with this functional give very good results.

ACKNOWLEDGMENTS

The author especially wishes to thank Dr. P. J. Roache and Dr. S. Steinberg for their support and encouragement.

REFERENCES

1. J. Hauser and C. Taylor (Eds.), *Computational Fluid Dynamics* (Pineridge Press, Swansea, UK, 1986).
2. S. Sengupta, J. Hauser, P. R. Eiseman, and J. F. Thompson (Eds.), *Computational Fluid Mechanics '88* (Pineridge Press, Swansea, UK, 1988).
3. A. M. Winslow, *J. Comput. Phys.* **2**, 149 (1967).
4. J. F. Thompson, F. Thames, and C. Mastin, *J. Comput. Phys.* **15**, 299 (1974).
5. J. F. Thompson, Z. U. A. Warsi, and C. W. Mastin, *Numerical Grid Generation: Foundations and Applications* (North-Holland, Elsevier Science, New York, 1985).
6. G. Ryskin and L. G. Leal, *J. Comput. Phys.* **50**, 71 (1983).
7. C. W. Mastin, in *Numerical Grid Generation*, edited by J. F. Thompson (North-Holland, New York, 1982), p. 31.
8. P. J. Roache and S. Steinberg, "A New Approach to Grid Generation Using a Variational Formulation," AIAA 7th Computation Fluid Dynamics Conference, Cinncinnati, OH, July 15–17, 1985.
9. C. W. Mastin, *J. Math. Anal. Appl.* **62**, 52 (1978).
10. S. Steinberg and P. Roache, *Numer. Methods Partial Diff. Eqs.* **2**, 71 (1986).
11. J. Brackbill and J. Saltzman, *J. Comput. Phys.* **46**, 342 (1982).
12. J. Castillo, S. Steinberg, and P. J. Roache, *Appl. Math. Comput.* **28**, 1 (1988).
13. J. Castillo, S. Steinberg, and P. J. Roache, *J. Comput. Appl. Math.* **20**, 127 (1987).
14. P. Knupp, "Surface Grid Generation in the Tangent Plane," Ecodynamics Research Associatiates, 1990 (unpublished).
15. J. Castillo, *SIAM J. Sci. Stat. Comput.* **12**, 454 (1991).
16. P. J. Roache, K. Salari, and S. Steinberg, *Commun. Appl. Numer. Methods* **7**, 345 (1991).
17. G. Liao, *Numer. Methods Partial Diff. Eqs.* **8**, 143 (1992).
18. P. J. Roache, Ecodynamics Research Associates, Albuquerque NM, private communication (1991).